INSTITUTE OF PHYSICS PUBLISHING PLASMA SOURCES SCIENCE AND TECHNOLOGY

Plasma Sources Sci. Technol. **10** (2001) 168–175 www.iop.org/Journals/ps PII: S0963-0252(01)20790-7

Density and temperature of N atoms in the afterglow of a microwave discharge measured by a two-photon laser-induced fluorescence technique

S Mazouffre[1], C Foissac[2], P Supiot[2], P Vankan[1], R Engeln[1], D C Schram[1] and N Sadeghi[3]

[1] Department of Applied Physics, Eindhoven University of Technology, PO Box 513, 5600 MB Eindhoven, The Netherlands
[2] Laboratoire de Génie des Procédés et d'Interactions Fluides Réactifs-Matériaux, Université des Sciences et Technologies de Lille, 59655 Villeneuve d'Ascq, France
[3] Laboratoire de Spectrométrie Physique, Université Joseph Fourier-Grenoble I and CNRS, BP 87, 38402 St Martin d'Heres cedex, France

Received 2 January 2001, in final form 5 March 2001

Abstract

Both the axial density and temperature profiles of ground-state nitrogen atoms have been measured in a microwave discharge and its afterglow in the presence of the so-called short-lived afterglow by means of two-photon absorption laser-induced fluorescence (TALIF). The temperature is obtained from the Doppler broadening of the spectral profile, after deconvolution with the laser profile. The N atom temperature decreases from about 1400 K in the end of the discharge zone to about 300 K in the downstream part of the afterglow. The sharp temperature decrease immediately behind the discharge zone can reasonably be explained by heat transfer to the flow tube wall. The absolute N atom density is obtained by calibrating the fluorescence yield with a TALIF signal from krypton atoms. The N density increases from 1.5×10^{21} m^{-3} in the discharge zone to about 3.5×10^{21} m^{-3} in the late afterglow. However, the N atom flux is conserved along the flow tube, indicating negligible consumption or production of N atoms in the short-lived afterglow.

1. Introduction

Due to the increasing number of plasma processes involving nitrogen, much effort is nowadays devoted to research on these systems. One of the main fields of application of such plasmas is surface treatment. Nitrogen-containing plasmas are widely used for the treatment of iron [1, 2], steel, and alloys [3–5]. The nitriding process is performed either within the discharge or in the afterglow. The aim is to improve the tribological and chemical properties (hardness, resistance to corrosion, and wear) of the surface of the material. This method has been successfully extended to a large set of metals (Ti [6], Al [7, 8], Cu, Au [1] etc), and non-metals (Si [9], III–V components [10]). Organic polymers (polyethylene, polypropylene, PET, PMMA, polycarbonate etc) are also treated using nitrogen plasma in order to modify the surface energy [11–13] and to favour adhesion. Furthermore, numerous applications are currently dedicated to thin-film deposition (polymers [14, 15], metals [16], and III–V compound nitrides [17], N_2 plasma-assisted pulsed laser deposition [18, 19]). It has been known for a long time that most of these plasma systems are characterized by a high nitrogen atom content. However, the role played by N atoms in the plasma kinetics and in the chemistry of the process itself is not yet perfectly understood. In view of all plasma processes involving nitrogen, it is therefore of importance to develop accurate and reliable diagnostic techniques to monitor the local properties of N atoms.

A traditional method to evaluate the N atom density in remote flowing afterglow systems is the use of NO titration [20]. This method is often used to calibrate the signal from emissions of the first positive (1^+) $N_2(B\,^3\Pi_g, v' = 10\text{–}12 \rightarrow A\,^3\Sigma_u^+, v'')$ transitions produced from atom–

atom recombination. Due to a near energy resonance, three-particle recombination of N atoms is likely to create nitrogen molecules in the $B\,^3\Pi_g$ ($v' = 10$–12) state. This preferential population of the high vibrational levels of $B\,^3\Pi_g$ leads to a strong departure from Boltzmann equilibrium in this state [21, 22]. The resulting emission on the 1^+ band is known as the Lewis–Rayleigh afterglow [20]. A simple monitoring of the band intensity, which is related to the square of the atom density, allows the determination of the N density after calibration by titration.

Nevertheless, the presence of the so-called short-lived afterglow (SLA) [23] no longer allows one to simply relate the $N_2(B\,^3\Pi_g, v' = 10$–$12)$ population to the N atom density, since in the SLA the strong 1^+ system emission can be caused by other processes apart from N recombination [24]. Some attempts to use the NO titration in the SLA have been performed [21, 25], but they were limited, without any insurance of the reliability of the measurements, to the end of the SLA. To the best of our knowledge the N atom density has never been directly measured in the SLA, which means no definitive conclusion can be drawn about its evolution and the possible role played by this species in the plasma kinetics. The possibility of probing ground-state atoms directly by two-photon absorption laser-induced fluorescence (TALIF) is well known and has been previously described by several authors [26, 27]. This diagnostic technique has already been applied successfully for the detection of N atoms in nitrogen plasma [28, 29]. The measurement of absolute N densities and temperature, however, has not yet been performed.

In this contribution, ground-state N atoms are probed by TALIF in a microwave discharge and its afterglow. The local temperature is extracted from the Doppler broadening of the spectral line, after deconvolution with the laser profile. A novel method is presented to determine the absolute N atom density, based on the recent experimental determination of the ratio of the two-photon excitation cross sections of N and krypton atoms. First, the experimental arrangement is described. Second, the method used to obtain the N atom temperature and density is explained in detail. Then the measured temperature and density profiles from the downstream part of the microwave discharge to the late afterglow are presented and discussed on the basis of kinetic processes. Finally, some conclusions are drawn.

2. Experimental arrangement

2.1. Plasma source

The microwave plasma reactor under consideration in this contribution has already been described in detail in previous works devoted to the monitoring of emission intensity [24] and of absolute density of $A\,^3\Sigma_u^+$ metastable nitrogen molecules [30] in this reactor. In short, the plasma is generated by a microwave coaxial resonant cavity operating at 433 MHz and mounted around a long pyrex tube (outside/inside diameter, 42/38 mm). The microwave generator delivers a maximal power of 400 W and a good impedance matching allows one to achieve less than 20 W of reflected power. The cavity is mounted on wheels and can therefore be displaced along the discharge tube. Spatial scans through the plasma can be made by moving the cavity relative to the intersection of the laser beam and the detection volume. The origin ($z = 0$) is taken to be the exit of the cavity. The positions of the different zones are the following: discharge end $z = 4$–5 cm; dark space minimum $z = 12$ cm; and pink afterglow maximum $z = 18$–19 cm.

The standard experimental conditions are: microwave power transmitted to the plasma $= 300$ W; N_2 flow rate $= 1.5$ standard litre per minute (slm); N_2 background pressure $= 440$ Pa.

2.2. Optical system and N atom detection

In the experiments reported here, ground-state nitrogen atoms are spatially probed by using a two-photon excitation laser-induced fluorescence technique [26, 27]. A scheme of the experimental set-up is depicted in figure 1. A 20 Hz Nd:YAG-pumped dye laser is operated around 620 nm. The output of the dye laser is frequency tripled resulting in 5 ns pulses of tunable horizontally polarized UV light around 207 nm, with a pulse energy up to 1 mJ and a bandwidth of approximately 0.25 cm^{-1} [31]. A Pellin–Broca prism is used to separate the UV beam from the remaining blue and red beams which are dumped. The UV laser beam, which has a diameter of about 2 mm, is then directed towards the discharge flow tube and subsequently focused by a MgF_2 lens ($f = 1$ m) into the tube through suprasil windows at Brewster angle.

As shown in figure 2, nitrogen atoms are excited with two 207 nm photons from the $2p\,^4S_{3/2}$ ground state to the $3p\,^4S_{3/2}$ state [28, 29, 32]. The excitation is monitored by detection of the 742–747 nm infrared fluorescence radiation which results from the spontaneous emission to the $3s\,^4P$ manifold. The excited-state fluorescence yield which originates from the detection volume is imaged perpendicular to both the laser beam and the flow tube axis by means of a lens ($f = 0.1$ m). The radiation is directed towards a gated photomultiplier tube (Hamamatsu R928). The continuous background light emitted by the plasma as well as the laser stray light is strongly reduced ($\times 100$) by a 10 nm FWHM interference filter centred at 742 nm.

The radial resolution of 8 mm is given by a slit mask located in front of the imaging mirror. The axial resolution of 0.3 mm is estimated from the diameter of the laser beam in the focus point. In view of the large focal distance of the lens used to focus the UV laser beam, its diameter is assumed to be constant along the slit length. The radial resolution may seem rather low, however no strong gradient is expected over such a distance. Therefore, we take advantage of a gain in fluorescence signal.

In order to assure no disturbance of the amount of produced fluorescence light, all parasitic effects which may affect the signal, such as three-photon ionization and amplified stimulated emission (ASE) [33], have to be avoided. At low laser intensity, i.e. far from the saturation regime, the fluorescence radiation yield S_{fluo} can be expressed as

$$S_{fluo} \propto n_N \sigma^{(2)} \frac{I_{laser}^2}{(h\nu)^2} A \tau f \qquad (1)$$

where $\sigma^{(2)}$ is the two-photon absorption cross section, $h\nu$ is the UV photon energy, n_N is the ground state nitrogen atom

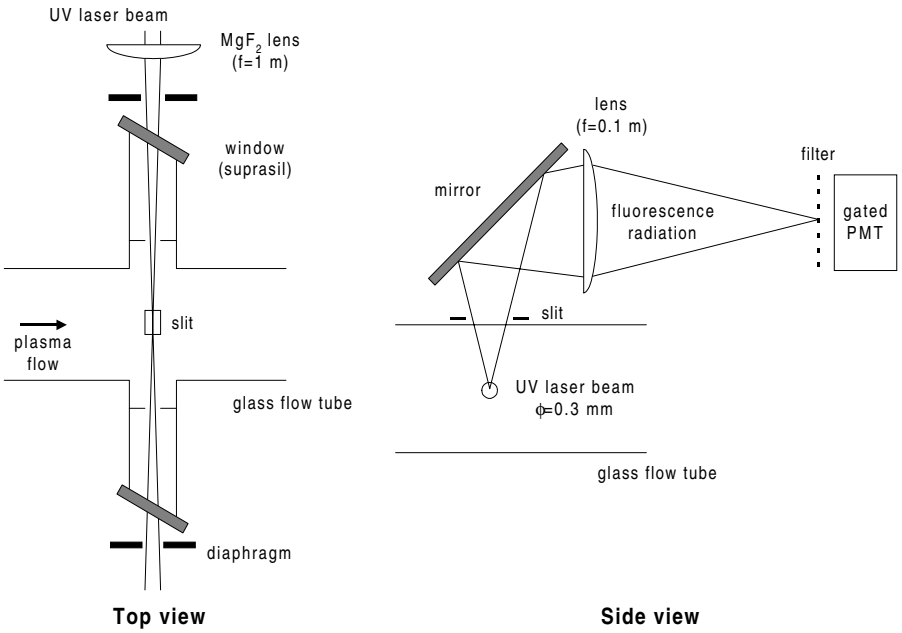

Figure 1. Sketch of the experimental TALIF set-up. The UV laser beam is focused at the centre of the plasma flow tube. The fluorescence radiation is detected at 90°. A filter is used to reduce the amount of plasma background light and laser stray light reaching the detector. A slit mask located in front of the imaging mirror defines the radial resolution (8 mm). To decrease the risk of ASE generation, both entrance and exit windows are positioned under Brewster's angle, and glass diaphragms are used to limit the diffusion of N atoms inside the two side arms.

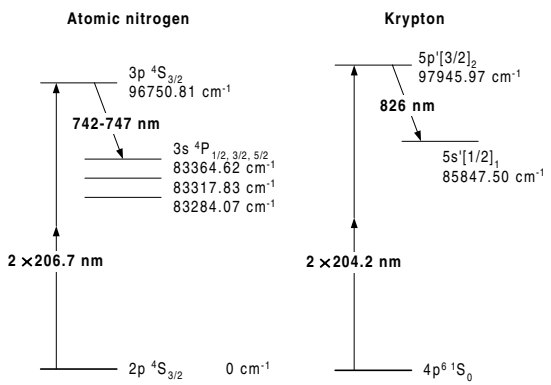

Figure 2. Simplified energy level diagram of atomic nitrogen and krypton indicating the excitation scheme and the observed fluorescence wavelengths. As can be seen, the two-photon excitation paths are very similar for N and Kr.

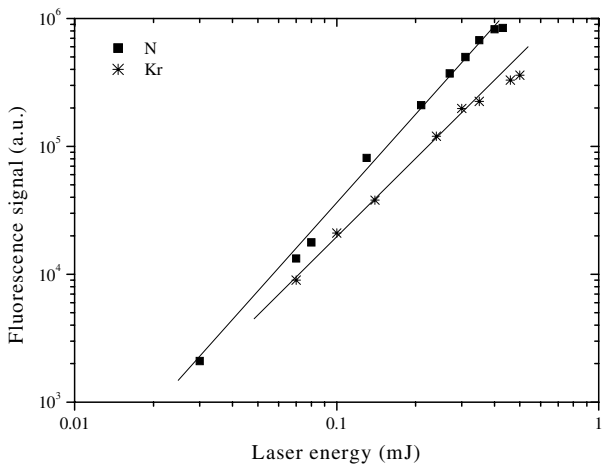

Figure 3. Log–log plot of the N atom fluorescence yield at resonance as a function of the 207 nm laser beam energy at the centre of the flow tube (squares). This measurement has been performed under standard conditions and at $z = 35$ cm. The slope of the line is found to be 2.3 ± 0.1. All measurements have been performed at 0.13 mJ. Also shown (stars) is the Kr atom fluorescence yield at resonance versus the 204 nm laser beam energy (10 Pa, 300 K). The slope of the line is 2.0 ± 0.1.

density, I_{laser} is the laser energy, A is the Einstein transition probability for spontaneous emission, τ is the lifetime of the excited level, and f is a factor which takes into account the geometry and the spectral response of the optical imaging and detection system. The excited-state lifetime τ accounts for both radiative processes and non-radiative processes, i.e. quenching. Therefore, it can be seen that, without any disturbing effects, the production of fluorescence radiation depends quadratically on the laser energy. In figure 3, a measured curve of the fluorescence signal at resonance versus the UV laser energy at the centre of the flow tube is shown for both N and Kr atoms. In the scanned energy range, we are in the so-called quadratic regime, and equation (1) holds. The fact that, in the case of N, the curve has a slope of 2.3 instead of 2 arises from a relatively low statistic combined with a weak fluorescence yield at low energy. All the measurements have been performed with a mean deposited laser energy around 130 μJ. One should note that since ASE generation scales with the integrated density of ground state N atoms along the laser beam, two glass diaphragms are used to prevent N atoms diffusing inside the two measurement arms, see figure 1. Positioning both entrance and exit windows under Brewster's angle also limits the ASE production.

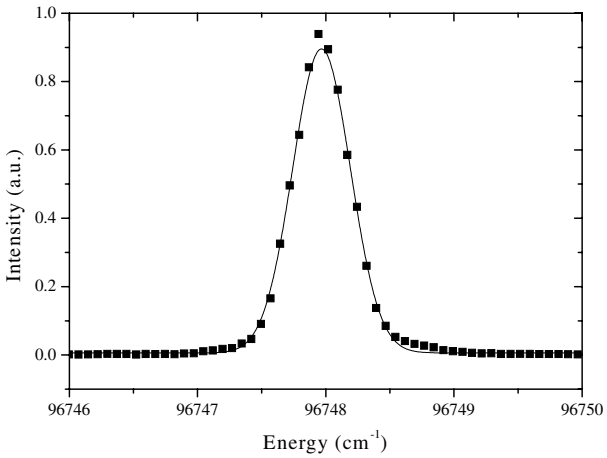

Figure 4. Spectral scan over the two-photon transition of atomic nitrogen ($z = 75$ cm, 0.4 slm N_2, 50 W, thus $T \approx T_{room}$). Also shown is a Gaussian fit. The small wing on the high-energy side arises from an slightly asymmetric laser profile. Assuming a Gaussian laser beam profile, the latter has a FWHM equal to 0.25 cm^{-1}.

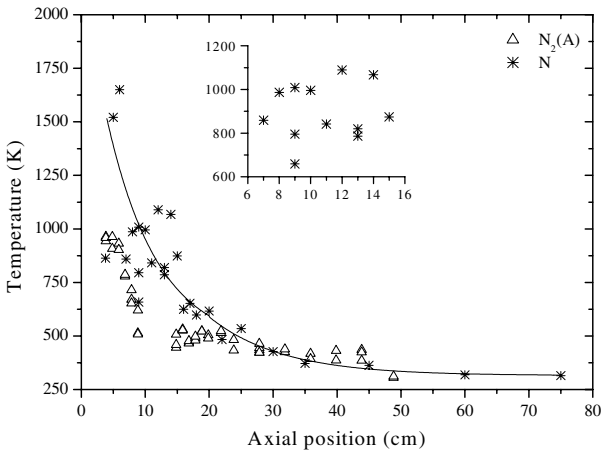

Figure 5. Nitrogen atom translational temperature (stars) and $N_2(A\,^3\Sigma_u^+, v' = 0)$ rotational temperature from [42] (triangles) as a function of the axial position. Both measurements have been performed under standard experimental conditions. The N_2(A) temperature is averaged along the discharge tube diameter whereas the N temperature is local. Also shown is the average N atom temperature (full curve) along the flow tube centreline (smoothed curve of the local N temperature).

3. Measured quantities

3.1. Translational temperature

The translational temperature of the ground state nitrogen atom is directly deduced from the Doppler broadening of the spectral line. In our experimental conditions, it can be shown that no other mechanism is responsible for the line broadening. However, it appears that, in view of the expected relatively low N atom temperature, the influence of the spectral profile of the UV laser beam cannot be neglected. The measured fluorescence spectral profile then corresponds to the convolution of the Doppler broadened atomic nitrogen line profile with the laser profile. Therefore, in order to be able to extract the Doppler linewidth from the measured spectral line, the shape of the laser spectral profile, as well as its bandwidth, have to be taken into account.

The spectral profile of the fundamental 620 nm laser at the exit of the dye laser is close to a Lorentzian in view of its 6 ns duration. Due to the nonlinear optical processes involved in the generation of the 207 nm photons needed in this experiment, the beam profile of the tripled radiation is modified in comparison with the beam profile of the dye laser. Because nonlinear effects only become significant at high energy, part of the energy contained in the wings of the fundamental and doubled light beams is not converted into UV light. This results in a UV laser beam profile which we assume to be Gaussian. In figure 4 the measured spectral profile used to determine the laser linewidth is presented, together with a Gaussian fit. Note that every point corresponds to the average of 256 laser shots. The shape of the measured profile is Gaussian, which strongly supports our assumption of a Gaussian UV beam profile, since both laser and Doppler profiles have comparable widths.

To determine the full width at half maximum (FWHM) of the laser profile, one can use a two-photon transition in krypton close to that used for atomic nitrogen, see figure 2. Thus one takes advantage of the small Doppler width of the Kr transition at room temperature ($m_{Kr} = 83$ amu). The existence of numerous Kr isotopes leads to a complex isotopic and hyperfine structure of the Kr line and, moreover, Kr is very sensitive to the Stark effect which can be induced by the laser beam electric field. The two effects may lead to an overestimated linewidth. Another solution is then to use cold N atoms. To create room-temperature N atoms, the discharge is operated under specific conditions: power = 50 W; N_2 flow rate = 0.4 slm; and pressure = 80 Pa. Furthermore, the measurements are performed far away from the plasma source ($z = 75$ cm) where the atoms are known to be at room temperature. The resulting N atom fluorescence profile is shown in figure 4. Because the Doppler width of the nitrogen transition $\Delta\nu_D$ can be calculated at 97 751 cm^{-1} ($\Delta\nu_D = 0.32$ cm^{-1} at 300 K), the laser profile width $\Delta\nu_L$ (i.e. the instrumental linewidth of the two-photon transition) can then be deduced from the measured Gaussian profile width $\Delta\nu_m$ by using the relation

$$\Delta\nu_D = \sqrt{\Delta\nu_m^2 - \Delta\nu_L^2}. \qquad (2)$$

At 300 K, the measured width (FWHM) of the TALIF spectral profile is equal to 0.4 cm^{-1}. Therefore, the laser spectral profile width $\Delta\nu_L$ (FWHM) is about 0.25 cm^{-1}. The uncertainty in the value of the measured laser beam spectral width is difficult to estimate. Nevertheless, the systematic error in the measured temperature is rather low as can be seen in figure 5. In the late afterglow, the measurements indicate a value close to room temperature as expected and in agreement with other studies. In the discharge zone, the spread in temperature is larger: $\Delta T \approx 300$ K. This results from a combination of a low signal-to-noise ratio because of the strong plasma emission and of a higher sensitivity to instabilities in the plasma flow.

3.2. Absolute atomic nitrogen density

The densities measured via laser-induced fluorescence are relative. In order to obtain absolute N atom number densities,

the fluorescence yield has to be calibrated, meaning that it has to be related to a well known amount of atomic nitrogen. This can be accomplished, for instance, by titration with NO [27, 28, 33] either directly in the discharge tube or using an independent source of N atoms as a flow tube reactor [20, 25, 34]. However, this method is cumbersome and the outcome may be difficult to interpret. A much easier way to calibrate the integrated laser-induced fluorescence spectral line is to use a well defined amount of krypton gas [35]. First, Kr has a two-photon excitation scheme very similar to N, as can be seen in figure 2. Second, the ratio of the Kr to N two-photon cross section has been recently measured [35]:

$$\frac{\sigma_{Kr}^{(2)}}{\sigma_{N}^{(2)}} = 0.67. \tag{3}$$

According to Niemi [35], due to the complexity of the measurement method, the error in the cross section ratio is in the order of 50%. The idea of using a noble gas to calibrate the fluorescence was first proposed by Goehlich *et al* [36]. Far from saturation, i.e. in the quadratic regime, the ground state atomic nitrogen density n_N is related to the krypton density n_{Kr} as follows:

$$n_N = n_{Kr} \frac{S_N}{S_{Kr}} \frac{\sigma_{Kr}^{(2)}}{\sigma_{N}^{(2)}} \left(\frac{\nu_N I_{Kr}}{\nu_{Kr} I_N} \right)^2 \frac{A_{Kr}\tau_{Kr}}{A_N \tau_N} \frac{\theta_{Kr}\zeta_{Kr}G_{Kr}}{\theta_N \zeta_N G_N} \tag{4}$$

where S is the fluorescence signal, i.e. the peak area, θ is the transmission of the optical detection system, ζ is the detector quantum efficiency, and G the detector amplification factor. All other parameters have been previously explained. The subscripts N and Kr refer to the TALIF measurement of atomic nitrogen and krypton, respectively. Identical geometry as well as identical laser beam shape and spectral profile are assumed in both cases.

The flow tube is filled with 10 Pa Kr at room temperature which corresponds to a Kr density of 2.4×10^{21} m^{-3}. A long-pass filter, $\theta = 0.95$ above 700 nm, is used to reduce the laser stray light impinging onto the photomultiplier tube (PMT). We were careful not to saturate the two-photon transition of Kr since the latter is easily subject to ASE generation [37]. The laser energy used to measure the Kr fluorescence profile is 130 μJ in the focus point (see figure 3). The calibration is performed at $z = 75$ cm.

A very fast PMT (Hamamatsu R5600P-01) with a single photon response of 1 ns [38] is used to measure the lifetime of the excited-state in both the N and the Kr cases. The lifetime of the krypton $5p'[3/2]_2$ state is found to be the radiative lifetime, as expected. Thus, τ_{Kr} is equal to 26.9 ns [39]. In our experimental conditions, the lifetime of the $3p\ ^4S_{3/2}$ state of N is shorter than its radiative lifetime, which is equal to 26.2 ± 1.5 ns [40]. Due to the quenching by N_2 molecules, the atomic nitrogen lifetime is found to be about 21.5 ns, which is roughly constant along the flow tube axis.

4. Results and discussion

4.1. N temperature profile

The N atom temperature T_N has been measured along the discharge tube axis from the discharge ($z = 4$ cm) to the late afterglow. The temperature profile is shown in figure 5, together with the rotational temperature T_r of the $N_2(A\ ^3\Sigma_u^+, v' = 0)$ species recently determined in this reactor [30, 41] by intra-cavity laser absorption spectroscopy (ICLAS) [42]. For $9 < z < 15$ cm, the $N_2(A)$ density is too low to enable the determination of T_r. In a pressure range of hundreds of pascals the neutral–neutral collision frequency is high enough (about 10^7 s^{-1}) to assure thermal equilibrium between the different heavy particles. Therefore, the N atom translational temperature represents the gas temperature.

In the region close to the cavity exit ($z < 15$ cm), despite the large fluctuations of T_N values (see section 3), the N temperature is seemingly higher than the $N_2(A)$ temperature. This arises directly from the fact that the TALIF technique allows one to obtain the local temperature (within the detection volume) whereas the ICLAS technique, being an absorption technique, delivers a temperature averaged along the discharge tube diameter. In view of the large radial temperature gradients behind the microwave cavity, the $N_2(A)$ temperature measured by ICLAS is expected to be lower than the N temperature measured along the tube axis as can be seen in figure 5. In the region $z > 20$ cm, the temperatures of N atoms and $N_2(A)$ molecules are in good agreement meaning that the radial temperature gradients are small. At large values of z ($z > 50$ cm), the gas temperature is constant and is approximately equal to room temperature.

The relatively high plasma temperature, around 1400 K, at the beginning of the discharge region is partly due the energy released during the creation of atomic nitrogen by electron impact dissociation of N_2 molecules via a repulsive state [43]. Indeed, this process leads to the creation of N atoms with an excess energy between 1 eV and 2 eV. The creation of several per cent of N atoms in the reactor can in that way increase significantly the gas temperature when the energy is redistributed by collisions. Nevertheless, other mechanisms favour a high temperature at the exit of the cavity. Heavy particles are heated by electron impact and energy is released due to vibration–translation (V–T) relaxation processes, to name but a few.

The total heat flux q at the exit of the cavity ($T = 1400$ K) can be estimated from the particle flux $\Phi (= 6.7 \times 10^{20}$ s$^{-1})$:

$$q = \tfrac{5}{2} \Phi k_B T \tag{5}$$

where k_B is the Boltzmann constant. We find that $q = 32$ W, which represents about 10% of the transmitted power. This value is reasonable since part of the energy is transferred to the wall and another part is converted into vibrational motion of molecules.

As can be seen in figure 5, the temperature drops quickly across the discharge zone and the dark space to reach approximately room temperature at about $z = 50$ cm. By solving the energy conservation equation ahead of the afterglow ($z < 20$ cm) it is possible to obtain information about the mechanism responsible for this temperature decrease. Assuming that there is no source term (no influence of the chemistry) and that the pressure is constant, and only considering heavy particles (the role played by electrons is negligible), the energy balance reads

$$\tfrac{5}{2} n_{N_2} k_B T \nabla \cdot \boldsymbol{u} = \nabla \cdot \boldsymbol{q} \tag{6}$$

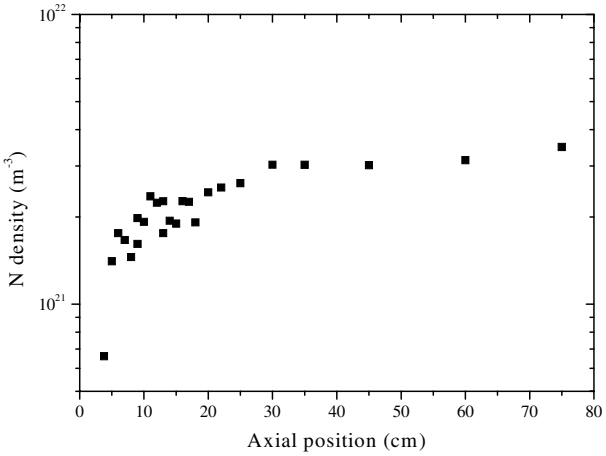

Figure 6. Absolute density of ground state nitrogen atoms as a function of the axial position measured in standard conditions. For $z < 10$ cm, due to the low signal-to-noise ratio, the error on the measurement point is large.

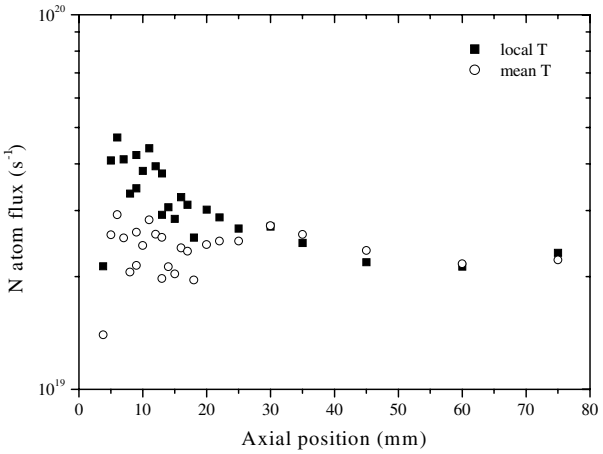

Figure 7. Nitrogen atom flux as a function of the axial position, calculated using the local temperature measured by TALIF (squares) and the radially average temperature measured by ICLAS (circles).

where $\boldsymbol{u}$ is the flow velocity and $\boldsymbol{q}$ is the particle heat flux given by Fourier's law for heat conduction: $\boldsymbol{q} = -\kappa \nabla T$ where κ is the heat conductivity. Nitrogen molecules N_2 are assumed to be the main component of the plasma. If we only consider radial losses, the foregoing equation reads in cylindrical coordinates (with a flat velocity profile):

$$\frac{5}{2} n k_B T \frac{\partial u}{\partial z} = \kappa \frac{1}{r} \frac{\partial}{\partial r} \left(r \frac{\partial T}{\partial r} \right). \tag{7}$$

The heat flux loss can be compared with heat transfer to the tube wall behind the cavity ($\Delta z = 20$ cm):

$$\frac{5}{4} n k_B T \frac{\Delta u}{\Delta z} = \kappa \frac{2}{R} \frac{\partial T}{\partial r}\bigg|_R. \tag{8}$$

The radial temperature profile is assumed to be linear and the temperature difference is taken to be 500 K from 0 to R. We have $\Delta u = 20$ m s^{-1} (see the next section) and $\kappa = 0.05$ W m^{-1} K^{-1} for N_2 at 800 K. The left-hand side of equation (8) is equal to 1.1×10^5 W m^{-3} and the right-hand side is equal to 1.3×10^5 W m^{-3}. In view of all assumptions, this can be considered as a good agreement between the two terms. Thus the temperature decrease throughout the discharge zone and the dark space can be reasonably explained by heat transfer to the tube wall. If we account for the tube cross section, the heat loss is found to be 140 W m^{-1}, which is in good agreement with the temperature drop. However, in this contribution we have only presented a first-order analysis, and a full solution of the energy balance is needed to confirm, for instance, that processes like vibrational relaxation do not influence the plasma temperature.

4.2. N atom density

The measured ground state atomic nitrogen density profile along the axis of the flow tube is presented in figure 6. The N density increases from the discharge to the late afterglow where it becomes constant (final value $\approx 3 \times 10^{21}$ m^{-3}, or about 13 Pa for the N atom partial pressure p_N).

Since the flow is subsonic, the flow velocity u is directly proportional to the local temperature because of flux conservation. If there is no loss and no significant creation of ground state N atoms in the course of the flow in the tube, the N atom flux is conserved. Using the perfect gas law the N flux ϕ_N reads

$$\phi_N = n_N \frac{k_B T}{p} \Phi. \tag{9}$$

where n_N is the atomic nitrogen density and p is the total static pressure. In other words, the partial static pressure of N atoms p_N is constant at every position (if full recirculation is assumed).

In figure 7 the flux of N atoms is plotted as a function of the axial position z. First, the N flux is calculated with equation (9), using the measured local N atom temperature. In this case, the N atoms flux is constant throughout the late afterglow ($z > 20$ cm) meaning that there is no loss and no creation of N atoms in this region. Disregarding the datapoint measured at $z = 4$ cm where the signal-to-noise ratio was relatively poor, the N atom flux decreases through the discharge zone and the dark space which indicates that N atoms are lost in the first centimetres of the discharge. However, in this calculation the radial gradient of temperature and velocity are not taken into account. In other words, the full squares in figure 7 represent merely the N forward flux. Second, the N atom flux is calculated with equation (9), using the $N_2(A)$ temperature measured by ICLAS [41] which we take to be equal to the N atom temperature. In such a way one accounts for the radial gradients, and thus the open circles represent the total N flux. As can be seen in figure 7, the total N flux is conserved from the discharge zone to the downstream part of the afterglow (disregarding the first point), meaning that N atoms are neither consumed nor produced behind the cavity. In order to substantiate this experimental fact, it is of importance to briefly consider all possible loss mechanisms for ground state N atoms.

Nitrogen atoms can recombine in volume to form excited N_2 molecules by a three-body recombination process:

$N(^4S) + N(^4S) + N_2 \rightarrow N_2(B\,^3\Pi_g, v'$; and other

triplet and quintet states) + N_2. (10)

The rate constant k_r for three-body recombination of N has been measured by Callede *et al* [44] as a function of the gas temperature T_g in the case of a N_2–Ar mixture, with Ar as a third body:

$$k_r = 6 \times 10^{-45} \exp\left[-0.4\left(\frac{T_g(\mathrm{K})}{296}\right)^2\right] (\mathrm{m}^6\ \mathrm{s}^{-1}). \quad (11)$$

The rate constant is expected to be almost unchanged when N_2 is used as a third body instead of Ar. The kinetic balance can then be expressed as follows:

$$\frac{\mathrm{d}n_N}{\mathrm{d}L} = -\frac{k_r}{u(L)} n_N^2 n_{N_2} \quad (12)$$

where u is the average flow speed calculated by taking the local temperature into account. The loss of N atoms calculated using equation (12) for high values of z, i.e. when the densities are the highest ($n_N = 3 \times 10^{21}$ m^{-3} and $n_{N_2} \approx 10^{23}$ m^{-3}) and the temperature is the lowest (T_g = room temperature) are found to be less than 10% per metre. Therefore, losses of N atoms by volume recombination can be neglected.

Ground-state N atoms can be transferred to an excited-state when colliding with N_2(A):

$$\mathrm{N}(^4\mathrm{S}) + \mathrm{N}_2(\mathrm{A}) \rightarrow \mathrm{N}(^2\mathrm{D}, ^2\mathrm{P}) + \mathrm{N}_2(\mathrm{X}, v') \quad (13)$$

with a rate coefficient $k_t = 4 \times 10^{-17}$ m^3 s^{-1} [43]. In our reactor, the mean density of N_2(A) molecules within the first 15 cm of the afterglow is of the order of 10^{17} m^{-3} [41] and $u(L) = 20$ m s^{-1}. Therefore, within this distance the loss of N atoms by reaction (13) is about 20% per metre. This would lead to 3% losses in the first 15 cm, which can be neglected.

Nitrogen atoms can also diffuse to the wall and recombine to form molecular nitrogen:

$$\mathrm{N}(^4\mathrm{S})_{gas} \xrightarrow{wall} \tfrac{1}{2}\mathrm{N}_{2\,gas}. \quad (14)$$

In cylindrical geometry and with a probability for wall recombination γ much smaller than unity, the N atom lifetime τ is given by [45, 46]

$$\tau = \tau_D + \frac{2R}{v_{th}\gamma} \quad (15)$$

where τ_D is the diffusion time, R is the tube radius, and v_{th} is the thermal speed. At $T = 900$ K, the diffusion time in the reactor is about 2.7 ms [30]. The probability γ for N atom recombination on Pyrex walls is very low: $\gamma \approx 10^{-5}$ [47]. With this value of γ, the lifetime of N atoms in this reactor would be 6 s, which is much larger than the residence time in the flow tube. However, in the discharge zone, the inside of the tube is relatively warm, about 500 K, and the surface is subject to intense charged particle bombardment, meaning that the value of γ can be significantly higher. With a value of γ as high as 10^{-2}, the N atom lifetime would be 10 ms. Considering a flow speed of 20 m s^{-1}, the density of N atoms would be reduced by 40% over 10 cm. However, outside the discharge zone γ must be much smaller than 10^{-2} and the diffusion loss should be negligible.

5. Conclusions

We have performed the measurement of the absolute density and translational temperature of ground state nitrogen atoms produced by a microwave discharge at 433 MHz by means of two-photon laser-induced fluorescence. An original calibration technique of the fluorescence yield based on a comparison with the rate of two-photon excitation of Kr has been presented.

The established N atom temperature profile is in agreement with measurements of the N_2(A) temperature. The temperature drop across the discharge zone and in the dark space can be reasonably explained by heat conduction to the tube wall. Along with the temperature decrease, the N atom density increases from the discharge to the late afterglow. This results in the fact that the N atom flux is conserved from the discharge zone to the downstream part of the afterglow, meaning that N atoms are neither consumed nor produced behind the cavity. In particular, this study definitely disclaims the possibility of significant N atom consumption within the short-lived afterglow. However, the radial N atom density and temperature profiles are needed to gain a better insight into the energy balance.

Acknowledgments

This work is part of the research program of the Netherlands Foundation for Fundamental Research on Matter (FOM). It is financially supported by the the Netherlands Organization for Scientific Research (NWO) as well as the Euratom foundation.

References

[1] Sanghera H K and Sullivan J L 1999 *Surf. Interface Anal.* **27** 678–90
[2] Camps E, Muhl S, Alvarez-Fregosz O, Juarez Islas J A, Olea O and Romero S 1999 *J. Vac. Sci. Technol.* **17** 2007–14
[3] Lebrun J P, Michel H and Gantois M 1972 *Mem. Sci. Rev. Metall.* **69** 727
[4] Ricard A 1989 *Rev. Phys. Appl.* **24** 251–6
[5] Walkowicz J, Smolik J and Miernik K 1999 *Surface Coating Technol.* **116–119** 361–6
[6] Okubo T, Kawamura H, Kusakabe K and Morooka S 1990 *J. Am. Ceram. Soc.* **73** 1150–2
[7] Nomato K I, Nishijima S and Mori H 1992 *Surf. Coating Technol.* **51** 157
[8] Duez N, Mutel B, Dessaux O, Goudmand P and Grimblot J 2000 *Surf. Coating Technol.* **125** 79–83
[9] Duez N, Mutel B, Vivien C, Gengembre L, Goudmand P, Dessaux O and Grimblot J 2001 *Surf. Sci.* in press
[10] Losurdo M, Capezzuto P, Bruno G, Leo G and Irene E A 1999 *J. Vac. Sci. Technol.* **17** 2194–201
[11] Liston E M 1989 *J. Adhesion* **30** 199–218
[12] Jama C, Dessaux O, Goudmand P, Gengembre L and Grimblot J 1992 *Surf. Interface Anal.* **18** 751–6
[13] Jama C, Quensierre J-D, Gengembre L, Moineau V, Grimblot J, Dessaux O and Goudmand P 1999 *Surf. Interface Anal.* **18** 751–6
[14] Callebert F, Supiot P, Asfardjani K, Goudmand P, Dessaux O, Laureyns J and Dhamelincourt P 1994 *J. Appl. Polym. Sci.* **52** 1595
[15] Baclez E, Mutel B, Dessaux O, Goudmand P, Grimblot J and Gengembre L 1997 *Thin Solid Film* **303** 156
[16] Stauden T, Eichhorn G, Cimalla V, Pezoldt J and Ecke G 1996

Diamond Rel. Mater. **5** 1210–13
[17] Ohtani T, Ihashi N and Matsumoto O 2000 *Trans. Mater. Res. Soc. Japan* **25** 47–50
[18] Caricato A P *et al* 1997 *Thin Solid Films* **307** 54–9
[19] Jama C, Dessaux O, Goudmand P, Soro J-M, Rats D and Van Stebut J 1999 *Surf. Coating Technol.* **116–119** 59–64
[20] Wright A N and Winkler C A 1968 *Active Nitrogen* (New York: Academic)
[21] Bockel S, Diamy A M and Ricard A 1995 *Surf. Coating Technol.* **74–75** 474–8
[22] Quensierre J D, Dupret C, Supiot P, Dessaux O and Goudmand P 1998 *Plasma Sources Sci. Technol.* **7** 491–8
[23] Supiot P, Dessaux O and Goudmand P 1995 *J. Phys. D: Appl. Phys.* **28** 1826–40
[24] Supiot P, Blois D, de Benedictis S, Dilecce G, Barj M and Chapput A 1999 *J. Phys. D: Appl. Phys.* **32** 1887–93
[25] Boisse-Laporte C, Chave-Normand C and Marec J 1997 *Plasma Sources Sci. Technol.* **6** 70
[26] Czarnetzki U, Miyazaki K, Kajiwara T, Muraoka K, Maeda M and Döbele H F 1994 *J. Opt. Soc. Am.* B **11** 2155
[27] Amorim J, Baravian G and Jolly J 2000 *J. Phys. D: Appl. Phys.* **33** R51
[28] Adams S F and Miller T A 1998 *Chem. Phys. Lett.* **295** 305
[29] Adams S F and Miller T A 2000 *Plasma Sources Sci. Technol.* **9** 248
[30] Foissac C, Campargue A, Kachanov A, Supiot P, Weirauch G and Sadeghi N 2000 *J. Phys. D: Appl. Phys.* **33** 2434
[31] Mazouffre S, Boogaarts M G H, Bakker I S J, van der Mullen J A M and Schram D C 1999 *Proc. 9th Laser-Aided Plasma Diagnostics (Lake Tahoe, CA)* p 320
[32] Boogaarts M G H, Brinkman G J, Mazouffre S, Döbele H F, van der Mullen J A M and Schram D C 1997 *Proc. 13th Int. Symp. on Plasma Chemistry (Beijing, China)* vol 2, p 529
[33] Amorim J, Baravian G, Touzeau M and Jolly J 1994 *J. Appl. Phys.* **76** 1487
[34] Setser D W 1979 *Reactive Intermediates in the Gas Phase* (New York: Academic)
[35] Niemi K, Schultz von der Gathen V and Dobele H F 2000 *Proc. Hakone 7 Symp. (Greifswald, Germany)* vol 1, p 199
[36] Goehlich A, Kawetzki T and Döbele H F 1998 *J. Chem. Phys.* **108** 9362
[37] Miller J C 1989 *Phys. Rev.* A **40** 6969
[38] van der Heijden H W P, Boogaarts M G H, Mazouffre S, van der Mullen J A M and Schram D C 2000 *Phys. Rev.* E **61** 4402
[39] Chang R S F, Horiguchi H and Setser D W 1980 *J. Chem. Phys.* **73** 778
[40] Bengtsson G J, Larsson J, Svanberg S and Wang D D 1992 *Phys. Rev.* A **45** 2712
[41] Sadeghi N, Foissac C and Supiot P 2001 *J. Phys. D: Appl. Phys.* submitted
[42] Campargue A, Chenevrier M and Stoekel 1990 *Spectrochem. Acta Rev.* **13** 69
[43] Guerra V and Loureiro J 1997 *Plasma Sources Sci. Technol.* **6** 361.
[44] Callede G, Deschamp J, Godart J L and Ricard A 1991 *J. Phys. D: Appl. Phys.* **24** 909
[45] Chantry P J 1987 *J. Appl. Phys.* **62** 1141
[46] Booth J-P and Sadeghi N 1991 *J. Appl. Phys.* **70** 611
[47] Yamashita T 1979 *J. Chem. Phys.* **70** 4248